Research Article | Vol. 25, No. 13 | 26 Jun 2017 | OPTICS EXPRESS 15093
Optics EXPRESS

Photothermal therapy of single cancer cells mediated by naturally created gold nanorod clusters

ZHIMIN CHEN,[1] HAIHUA FAN,[1] JINXIANG LI,[1] SHAOLONG TIE,[2] AND SHENG LAN[1*]

[1]*Guangdong Provincial Key Laboratory of Nanophotonic Functional Materials and Devices, School of Information and Optoelectronic Science and Engineering, South China Normal University, Guangzhou 510006, China*
[2]*School of Chemistry and Environment, South China Normal University, Guangzhou 510006, China*
**slan@scnu.edu.cn*

Abstract: Gold nanorods (GNRs) are generally considered to be nontoxic to normal and cancer cells. They are usually accumulated at lysosomes after entering into cells, forming GNR clusters in which strong plasmonic coupling between GNRs is expected. We investigated the photothermal therapy of single cancer cells by exploiting the significantly enhanced two-photon-induced absorption of GNR clusters naturally created in the lysosomes of cancer cells. It was revealed numerically that the plasmonic coupling between GNRs in GNR clusters can effectively enhance the photothermal conversion efficiency. As a result, the thermal damage of single cancer cells can be induced by using pulse energy as low as ~70 pJ. In experiments, the locations of GNR clusters can be accurately determined through the detection of the two-photon-induced luminescence, which is also significantly enhanced, by using a confocal laser scanning microscope. The photothermal therapy was conducted by focusing femtosecond laser light on the targeted GNR clusters, generating bubbles and deforming cell membranes. The photothermal therapy proposed in this work can lead to the rapid and acute injury of single cancer cells. The dependence of the apoptosis time on the pulse energy of femtosecond laser light was also examined. Our findings suggest a novel strategy for the photothermal therapy of single cancer cells with ultralow energy.

OCIS codes: (160.4236) Nanomaterials; (190.4180) Multiphoton processes; (140.3538) Lasers, pulsed; (190.4870) Photothermal effects.

References and links

1. J. Shi, P. W. Kantoff, R. Wooster, and O. C. Farokhzad, "Cancer nanomedicine: progress, challenges and opportunities," Nat. Rev. Cancer **17**(1), 20–37 (2017).
2. W. Tao, X. Zhu, X. Yu, X. Zeng, Q. Xiao, X. Zhang, X. Ji, X. Wang, J. Shi, H. Zhang, and L. Mei, "Black phosphorus nanosheets as a robust delivery platform for cancer theranostics," Adv. Mater. **29**(1), 1603276 (2017).
3. S. S. Chou, B. Kaehr, J. Kim, B. M. Foley, M. De, P. E. Hopkins, J. Huang, C. J. Brinker, and V. P. Dravid, "Chemically exfoliated MoS_2 as near-infrared photothermal agents," Angew. Chem. Int. Ed. Engl. **52**(15), 4160–4164 (2013).
4. J. Shi, Z. Xiao, N. Kamaly, and O. C. Farokhzad, "Self-assembled targeted nanoparticles: evolution of technologies and bench to bedside translation," Acc. Chem. Res. **44**(10), 1123–1134 (2011).
5. Z. Xiao, C. Ji, J. Shi, E. M. Pridgen, J. Frieder, J. Wu, and O. C. Farokhzad, "DNA self-assembly of targeted near-infrared-responsive gold nanoparticles for cancer thermo-chemotherapy," Angew. Chem. Int. Ed. Engl. **51**(47), 11853–11857 (2012).
6. J. Wang, G. Zhu, M. You, E. Song, M. I. Shukoor, K. Zhang, M. B. Altman, Y. Chen, Z. Zhu, C. Z. Huang, and W. Tan, "Assembly of aptamer switch probes and photosensitizer on gold nanorods for targeted photothermal and photodynamic cancer therapy," ACS Nano **6**(6), 5070–5077 (2012).
7. J. Song, X. Yang, O. Jacobson, P. Huang, X. Sun, L. Lin, X. Yan, G. Niu, Q. Ma, and X. Chen, "Ultrasmall gold nanorod vesicles with enhanced tumor accumulation and fast excretion from the body for cancer therapy," Adv. Mater. **27**(33), 4910–4917 (2015).
8. Y. Wang, K. C. L. Black, H. Luehmann, W. Li, Y. Zhang, X. Cai, D. Wan, S. Y. Liu, M. Li, P. Kim, Z. Y. Li, L. V. Wang, Y. Liu, and Y. Xia, "Comparison study of gold nanohexapods, nanorods, and nanocages for

#294809 https://doi.org/10.1364/OE.25.015093
Journal © 2017 Received 28 Apr 2017; revised 17 Jun 2017; accepted 17 Jun 2017; published 21 Jun 2017

Optics EXPRESS

photothermal cancer treatment," ACS Nano **7**(3), 2068–2077 (2013).
9. P. Huang, L. Bao, C. Zhang, J. Lin, T. Luo, D. Yang, M. He, Z. Li, G. Gao, B. Gao, S. Fu, and D. Cui, "Folic acid-conjugated silica-modified gold nanorods for X-ray/CT imaging-guided dual-mode radiation and photo-thermal therapy," Biomaterials **32**(36), 9796–9809 (2011).
10. M. Sun, F. Liu, Y. Zhu, W. Wang, J. Hu, J. Liu, Z. Dai, K. Wang, Y. Wei, J. Bai, and W. Gao, "Salt-induced aggregation of gold nanoparticles for photoacoustic imaging and photothermal therapy of cancer," Nanoscale **8**(8), 4452–4457 (2016).
11. Z. Li, H. Huang, S. Tang, Y. Li, X. F. Yu, H. Wang, P. Li, Z. Sun, H. Zhang, C. Liu, and P. K. Chu, "Small gold nanorods laden macrophages for enhanced tumor coverage in photothermal therapy," Biomaterials **74**, 144–154 (2016).
12. L. Pan, J. Liu, and J. Shi, "Nuclear-targeting gold nanorods for extremely low NIR activated photothermal therapy," ACS Appl. Mater. Interfaces **9**(19), 15952–15961 (2017).
13. M. Aioub, S. R. Panikkanvalappil, and M. A. El-Sayed, "Platinum-coated gold nanorods: efficient reactive oxygen scavengers that prevent oxidative damage toward healthy, untreated cells during plasmonic photothermal therapy," ACS Nano **11**(1), 579–586 (2017).
14. M. Pérez-Hernández, P. Del Pino, S. G. Mitchell, M. Moros, G. Stepien, B. Pelaz, W. J. Parak, E. M. Gálvez, J. Pardo, and J. M. de la Fuente, "Dissecting the molecular mechanism of apoptosis during photothermal therapy using gold nanoprisms," ACS Nano **9**(1), 52–61 (2015).
15. E. D. Onal and K. Guven, "Plasmonic photothermal therapy in third and fourth biological windows," J. Phys. Chem. C **121**(1), 684–690 (2017).
16. J. L. Li, D. Day, and M. Gu, "Ultra-low energy threshold for cancer photothermal therapy using transferrin-conjugated gold nanorods," Adv. Mater. **20**(20), 3866–3871 (2008).
17. X. Wu, J. Y. Chen, A. Brech, C. Fang, J. Wang, P. J. Helm, and Q. Peng, "The use of femto-second lasers to trigger powerful explosions of gold nanorods to destroy cancer cells," Biomaterials **34**(26), 6157–6162 (2013).
18. V. P. Pattani, J. Shah, A. Atalis, A. Sharma, and J. W. Tunnell, "Role of apoptosis and necrosis in cell death induced by nanoparticle-mediated photothermal therapy," J. Nanopart. Res. **17**(1), 20–31 (2015).
19. W. I. Choi, J. Y. Kim, C. Kang, C. C. Byeon, Y. H. Kim, and G. Tae, "Tumor regression *in vivo* by photothermal therapy based on gold-nanorod-loaded, functional nanocarriers," ACS Nano **5**(3), 1995–2003 (2011).
20. J. Nam, N. Won, H. Jin, H. Chung, and S. Kim, "pH-Induced aggregation of gold nanoparticles for photothermal cancer therapy," J. Am. Chem. Soc. **131**(38), 13639–13645 (2009).
21. M. A. El-Sayed, A. A. Shabaka, O. A. El-Shabrawy, N. A. Yassin, S. S. Mahmoud, S. M. El-Shenawy, E. Al-Ashqar, W. H. Eisa, N. M. Farag, M. A. El-Shaer, N. Salah, and A. M. Al-Abd, "Tissue distribution and efficacy of gold nanorods coupled with laser induced photoplasmonic therapy in ehrlich carcinoma solid tumor model," PLoS One **8**(10), e76207 (2013).
22. Y. S. Wang, D. Shao, L. Zhang, X. L. Zhang, J. Li, J. Feng, H. Xia, Q. S. Huo, W. F. Dong, and H. B. Sun, "Gold nanorods-silica Janus nanoparticles for theranostics," Appl. Phys. Lett. **106**(17), 173705 (2015).
23. S. Bhana, R. O'Connor, J. Johnson, J. D. Ziebarth, L. Henderson, and X. Huang, "Photosensitizer-loaded gold nanorods for near infrared photodynamic and photothermal cancer therapy," J. Colloid Interface Sci. **469**, 8–16 (2016).
24. C. Ungureanu, R. Kroes, W. Petersen, T. A. M. Groothuis, F. Ungureanu, H. Janssen, F. W. B. van Leeuwen, R. P. H. Kooyman, S. Manohar, and T. G. van Leeuwen, "Light interactions with gold nanorods and cells: implications for photothermal nanotherapeutics," Nano Lett. **11**(5), 1887–1894 (2011).
25. J. L. Li and M. Gu, "Surface plasmonic gold nanorods for enhanced two-photon microscopic imaging and apoptosis induction of cancer cells," Biomaterials **31**(36), 9492–9498 (2010).
26. W. B. Zhou, X. S. Liu, and J. Ji, "More efficient NIR photothermal therapeutic effect from intracellular heating modality than extracellular heating modality: an in vitro study," J. Nanopart. Res. **14**(9), 1128–1144 (2012).
27. X. M. Zhu, C. Fang, H. Jia, Y. Huang, C. H. K. Cheng, C. H. Ko, Z. Chen, J. Wang, and Y. X. J. Wang, "Cellular uptake behaviour, photothermal therapy performance, and cytotoxicity of gold nanorods with various coatings," Nanoscale **6**(19), 11462–11472 (2014).
28. L. Chen, G. C. Li, G. Y. Liu, Q. F. Dai, S. Lan, S. L. Tie, and H. D. Deng, "Sensing the moving direction, position, size, and material type of nanoparticles with the two-photon-induced luminescence of a single gold nanorod," J. Phys. Chem. C **117**(39), 20146–20153 (2013).
29. P. Zijlstra, J. W. M. Chon, and M. Gu, "Five-dimensional optical recording mediated by surface plasmons in gold nanorods," Nature **459**(7245), 410–413 (2009).
30. T. Zhao, X. Shen, L. Li, Z. Guan, N. Gao, P. Yuan, S. Q. Yao, Q. H. Xu, and G. Q. Xu, "Gold nanorods as dual photo-sensitizing and imaging agents for two-photon photodynamic therapy," Nanoscale **4**(24), 7712–7719 (2012).
31. Z. Zhang, L. Wang, J. Wang, X. Jiang, X. Li, Z. Hu, Y. Ji, X. Wu, and C. Chen, "Mesoporous silica-coated gold nanorods as a light-mediated multifunctional theranostic platform for cancer treatment," Adv. Mater. **24**(11), 1418–1423 (2012).
32. H. Chen, L. Shao, T. Ming, Z. Sun, C. Zhao, B. Yang, and J. Wang, "Understanding the photothermal conversion efficiency of gold nanocrystals," Small **6**(20), 2272–2280 (2010).
33. B. D. Chithrani, A. A. Ghazani, and W. C. W. Chan, "Determining the size and shape dependence of gold nanoparticle uptake into mammalian cells," Nano Lett. **6**(4), 662–668 (2006).
34. Y. Qiu, Y. Liu, L. Wang, L. Xu, R. Bai, Y. Ji, X. Wu, Y. Zhao, Y. Li, and C. Chen, "Surface chemistry and

Optics EXPRESS

aspect ratio mediated cellular uptake of Au nanorods," Biomaterials **31**(30), 7606–7619 (2010).
35. A. M. Alkilany, P. K. Nagaria, C. R. Hexel, T. J. Shaw, C. J. Murphy, and M. D. Wyatt, "Cellular uptake and cytotoxicity of gold nanorods: molecular origin of cytotoxicity and surface effects," Small **5**(6), 701–708 (2009).
36. A. Malugin, H. Ghandehari, "Cellular uptake and toxicity of gold nanoparticles in prostate cancer cells: a comparative study of rods and spheres," J. Appl. Toxicol. **30**(3), 212–217 (2010).
37. S. Shen, H. Tang, X. Zhang, J. Ren, Z. Pang, D. Wang, H. Gao, Y. Qian, X. Jiang, and W. Yang, "Targeting mesoporous silica-encapsulated gold nanorods for chemo-photothermal therapy with near-infrared radiation," Biomaterials **34**(12), 3150–3158 (2013).
38. C. Ungureanu, R. Kroes, W. Petersen, T. A. M. Groothuis, F. Ungureanu, H. Janssen, F. W. B. van Leeuwen, R. P. H. Kooyman, S. Manohar, and T. G. van Leeuwen, "Light interactions with gold nanorods and cells: implications for photothermal nanotherapeutics," Nano Lett. **11**(5), 1887–1894 (2011).
39. J. X. Li, Y. Xu, Q. F. Dai, S. Lan, and S. L. Tie, "Manipulating light–matter interaction in a gold nanorod assembly by plasmonic coupling," Laser Photonics Rev. **10**(5), 826–834 (2016).
40. F. Kim, J. H. Song, and P. Yang, "Photochemical synthesis of gold nanorods," J. Am. Chem. Soc. **124**(48), 14316–14317 (2002).
41. K. S. Yee, "Numerical solution of inital boundary value problems involving Maxwell's equations in isotropic media," IEEE Trans. Antenn. Propag. **14**(3), 302–307 (1966).
42. P. Yang and K. N. Liou, "Finite-difference time domain method for light scattering by small ice crystals in three-dimensional space," J. Opt. Soc. Am. A **13**(10), 2072–2085 (1996).
43. S. Viarbitskaya, A. Teulle, R. Marty, J. Sharma, C. Girard, A. Arbouet, and E. Dujardin, "Tailoring and imaging the plasmonic local density of states in crystalline nanoprisms," Nat. Mater. **12**(5), 426–432 (2013).
44. P. Ghenuche, S. Cherukulappurath, T. H. Taminiau, N. F. van Hulst, and R. Quidant, "Spectroscopic mode mapping of resonant plasmon nanoantennas," Phys. Rev. Lett. **101**(11), 116805 (2008).
45. T. Haug, P. Klemm, S. Bange, and J. M. Lupton, "Hot-electron intraband luminescence from single hot spots in noble-metal nanoparticle films," Phys. Rev. Lett. **115**(6), 067403 (2015).
46. X. F. Jiang, Y. Pan, C. Jiang, T. Zhao, P. Yuan, T. Venkatesan, and Q. H. Xu, "Excitation nature of two-photon photoluminescence of gold nanorods and coupled gold nanoparticles studied by two-pulse emission modulation spectroscopy," J. Phys. Chem. Lett. **4**(10), 1634–1638 (2013).
47. P. Biagioni, M. Celebrano, M. Savoini, G. Grancini, D. Brida, S. Mátéfi-Tempfli, M. Mátéfi-Tempfli, L. Duò, B. Hecht, G. Cerullo, and M. Finazzi, "Dependence of the two-photon photoluminescence yield of gold nanostructures on the laser pulse duration," Phys. Rev. B **80**(4), 045411 (2009).
48. H. Wang, T. B. Huff, D. A. Zweifel, W. He, P. S. Low, A. Wei, and J. X. Cheng, "*In vitro* and *in vivo* two-photon luminescence imaging of single gold nanorods," Proc. Natl. Acad. Sci. U.S.A. **102**(44), 15752–15756 (2005).

1. Introduction

In recent years, rapid development in the synthesis and characterization of nanomaterials has stimulated the use of various nanomaterials as cancer nanomedicines [1], including novel two-dimensional materials that have received intensive studies [2,3]. In particular, self-assembled targeted nanoparticles have been developed for safer and more effective therapeutic or imaging applications [4]. For photothermal therapy, however, much effort has been devoted to metallic nanoparticles because they can strongly absorb electromagnetic waves of different frequencies, leading to a rapid temperature rise [5–9].

Owing to their superior optical response, thermal conductivity and chemical stability, gold nanoparticles/nanostructures of different sizes and shapes have been considered as one of the most important materials for photothermal therapy [10–15]. For example, Sun et al. found that the salt-induced aggregation of gold nanoparticles in biological media creates highly efficient and biocompatible photothermal transducers for photothermal therapy and photothermal/photo-acoustic imaging of cancer cells [10]. In addition, Li et al. observed that small gold nanorod (GNR) laden macrophages exhibit enhanced tumor coverage in photothermal therapy [11]. Pan et al. revealed that extremely low NIR activated photothermal therapy can be realized by using nuclear-targeting GNRs [12]. More interestingly, Aioub et al. demonstrated that platinum-coated GNRs act as efficient reactive oxygen scavengers that prevent oxidative damage toward healthy cells during plasmonic photothermal therapy [13].

In general, electromagnetic waves in different spectral ranges, such as X-ray [9], white light [6], and near infrared laser [7,8,16–24], can be employed in photothermal therapy. However, near infrared laser is considered as the most suitable one because of the low attenuation of laser energy when passing through tissues or cells [6,8]. In practice, both unfocused [9,19,20] and focused [16,17,25] laser beams have been used in the photothermal

Optics EXPRESS

therapy of cells. The photothermal conversion efficiency of metallic nanoparticles is generally considered as a key issue because the temperature rise necessary for photothermal therapy can be induced by using low pulse energy if metallic nanoparticles with high photothermal conversation efficiency are employed. In general, small nanoparticles possess higher photothermal conversion efficiency because of their low scattering cross sections. The low absorption cross sections can be compensated by increasing the concentration of nanoparticles, which can be realized by increasing the uptake of nanoparticles through for example surface modification [26,27].

In the past decade, GNRs have been the focus of many studies such as nanoscale sensing, optical data storage, bioimaging, drug delivery, and photothermal therapy [28–31] owing to their superior optical properties and chemical stability. The existence of longitudinal surface plasmon resonances (LSPRs) with significantly enhanced electric field and flexible tunability makes them a promising candidate in bioimaging, biomedicine and photothermal therapy. The photothermal conversion efficiency of GNRs has been investigated and it was found that smaller GNRs possess higher photothermal conversion efficiency because the scattering cross sections of small GNRs are negligible [32]. On the other hand, the cytotoxicity of GNRs has been extensively studied and GNRs with different aspect ratios are generally nontoxic to normal cells [33–36]. This characteristic makes them a suitable nanomaterial for photothermal therapy.

So far, the GNR-based photothermal therapy is generally performed for a large number of cells and there is no study on the photothermal therapy of single cells which is interesting from the viewpoint of both fundamental research and practical application. In addition, the high pulse energy used in the previous studies may lead to the damage of normal cells and how to realize photothermal therapy with ultralow energy has become an important issue to be solved.

It has been known that GNRs are naturally accumulated in the lysosomes after entering into cells [37,38], creating GNR clusters in which strong plasmonic coupling between GNRs may exist. The existence of strong plasmonic coupling would change dramatically the linear and nonlinear absorption of GNR clusters, significantly enhancing the two-photon-induced absorption (TPA) and two-photon-induced luminescence (TPL) of GNR clusters [39]. Therefore, such naturally-formed GNR clusters can be employed to realize the photothermal therapy of single cells with ultralow energy.

In this work, we investigated the photothermal therapy of single cancer cells mediated by GNR clusters naturally formed in the lysosomes of cancer cells. The effect of plasmonic coupling between GNRs in GNR clusters was numerically studied based on the finite-difference time-domain (FDTD) method. It was found that the TPA and TPL of the GNR clusters are significantly enhanced, which in turn reduces the pulse energy used in the photothermal therapy of single cancer cells. We used the TPL emitted by the GNR clusters to accurately locate the positions of the GNR cluster with the strongest TPA and performed photothermal therapy by focusing femtosecond (fs) laser light on the targeted GNR cluster. The dependence of the apoptosis time on the irradiation time and energy was also examined.

2. Experimental details and numerical methods

The GNRs used in the experiments were synthesized by using a modified seedless method which is similar to that described previously [40]. The as-prepared GNRs were then stabilized by polyethylene glycol (PEG). The LSPRs of the GNRs were characterized by measuring the UV-Vis-NIR absorption spectra. The morphology of the GNRs was examined by using transmission electron microscopy (TEM).

The cancer cells used in the photothermal therapy were human liver hepatocellular carcinoma (HepG2). They were cultured in a humidified incubator at 37°C with an atmosphere containing 5% CO_2. The culture medium was composed of 89% Dulbecco's Modified Eagle Medium (DMEM), 10% fetal bovine serum and 1% penicillin/streptomycin.

Optics EXPRESS

The cytotoxicity of GNRs *in vitro* was evaluated against HepG2 cells by using the Thiazolyl Blue Tetrazolium Bromide (MTT) assay. In brief, approximately 4000 cells per well were pre-cultured in a plate with 96 wells for 12 hours. The cells were then incubated with 100-mL medium containing GNRs for 24 hours. After incubation, 10-μL MTT (5 mg/mL) was added into each well, followed by an additional incubation of 4 hours. Then, the solution was replaced by 100-mL Dimethyl Sulphoxide (DMSO) to dissolve the formed formazan crystals. Cell viability (%) was calculated by comparing the absorbance of the testing wells at 570 nm with that of the control wells containing untreated cells.

For cellular uptake studies, HepG2 cells were seeded in cell culture flasks (~25 cm^2) and allowed to settle overnight. Then, they were incubated with culture media containing GNRs with different concentrations of 0, 52.2, 78.3, 104.4, 130.5 and 156.6 pM at 37 °C and 5% CO_2 for 24 hours. After that, the culture media were removed and the cells were washed three times with phosphate buffered saline (PBS). The cells were lifted by trypsin (0.025%; Gibco, Invitrogen, Belgium) and pelleted by centrifugation. For the measurement of the gold (Au) concentration, the cell pellets were dispersed in 1-mL PBS to determine cell amount. Cell suspension was dissolved in 2.5-mL aqua regia and modulated into a 10-mL solution after driving acid. The concentration of Au is analyzed by inductively coupled plasma-mass spectrometry (ICP-MS) (ICAP-qc, Thermo Fisher) [26]. The number of GNRs within a single cell can be derived from the volume (10 mL) and GNR concentrations (55–155 pM) of the culture media, the volume (1.62×10^{-18} cm^3) and mass (3.14×10^{-17} g) of a single GNR, the concentrations of Au measured by ICP-MS, and the amount of cells.

Apart from ICP-MS, the cellular uptake was also examined by using TEM observation. In this case, HepG2 cells were seeded in cell culture flasks (~25 cm^2) and allowed to settle overnight. Next, they were incubated with the culture media containing GNRs of 0 or 104.4 pM for 24 hours in a humidified incubator (37°C, 5% CO_2). After removing the culture media, the cells were washed three times with PBS, separated from culture flasks with cell scraper, and pelleted by centrifugation. Finally, they were fixed in 1% osmic acid for 20 minutes and cut into cell slices for TEM observation at an acceleration voltage of 120 kV.

The photothermal therapy experiments were carried out by using either an inverted microscope (Axio Observer A1, Zeiss) or a confocal laser scanning microscope (TCS-SP5, Leica). In the former case, the femtosecond (fs) laser light from a Ti: sapphire oscillator (Mira 900S, Coherent) with a repetition rate of 76 MHz was focused on the targeted cell by using a 60 × objective lens. The diameter of the laser spot was estimated to be ~1.8 μm. The pulse energy of 1 pJ corresponds to laser fluence of 3.93×10^{-2} mJ/cm^2. The TPL emitted by the GNR clusters was collected by the same objective lens and directed to a spectrometer for analysis. The TPL imaging of the cell was carried out by using a three-dimensional positioning system (P-563.3CD, Physik Instruments). For the photothermal therapy performed by using a confocal laser scanning microscope, the cells were plated in a confocal culture dish (5×10^3 cells/well) and incubated for 12 hours. Then, they were incubated by using a culture medium containing 104.4-pM GNRs for 24 hours. After that, the cells were washed by PBS for three times and observed in DMEM under the confocal laser scanning microscope. The wavelength and repetition rate of the fs laser light were 800 nm and 76 MHz. The pulse energies used for scanning and photothermal therapy were chosen to be 35 and 420 pJ, respectively. The diameter of the laser spot size was estimated to be ~1.0 μm.

The FDTD software developed by Lumerical Solutions, Inc. (http://www.lumerical.com) was employed to simulate the distribution of electric field in GNR clusters from which the linear and nonlinear absorption spectra of the GNR clusters can be derived [41,42]. In the FDTD simulations, non-uniform grids with the smallest grid of 0.2 nm and perfectly matched layer condition were employed. The COMSOL multiphysics software developed by Comsol Inc. (http://www.comsol.com) was employed to simulate the temperature distribution inside the GNR clusters.

Optics EXPRESS

3. Results and discussion

3.1 Linear and nonlinear absorption of GNR clusters

It has been known that GNRs are usually accumulated at lysosomes, forming GNR clusters after entering into cells. Distinct from isolated GNRs, there exists strong plasmonic coupling between GNRs in such GNR clusters. As a result, the linear and nonlinear absorption (i.e., TPA) will be significantly modified owing to the existence of strong plasmonic coupling. Since photothermal conversion efficiency is closely related to the linear and nonlinear absorption, it is necessary to investigate the modification in the linear and nonlinear absorption induced by the plasmonic coupling presented in GNR clusters.

In Fig. 1, we show schematically the physical model used to study the effects of plasmonic coupling on the linear and nonlinear absorption of GNR clusters. In Fig. 1(a), 100 GNRs with random orientations and positions are enclosed in a box with a volume of 300 × 300 × 300 nm^3. The background is water with a refractive index of 1.33. The length and diameter of GNRs are chosen to be 34 and 8 nm, respectively. In this case, the mean distance between GNRs is much larger than the length of GNRs and the coupling between GNRs is negligible. In contrast, strong coupling is expected for the GNR cluster in which 100 GNRs are enclosed in a box with a smaller volume of 200 × 200 × 200 nm^3, as shown in Fig. 1(b). In this case, the mean separation between GNRs becomes comparable to the length of GNRs, which is typical for the GNR clusters observed in the lysosomes of cells, as will be shown later. Therefore, we first compare the linear and nonlinear absorption of the two GNR clusters without and with plasmonic coupling, as shown in Figs. 1(a) and 1(b).

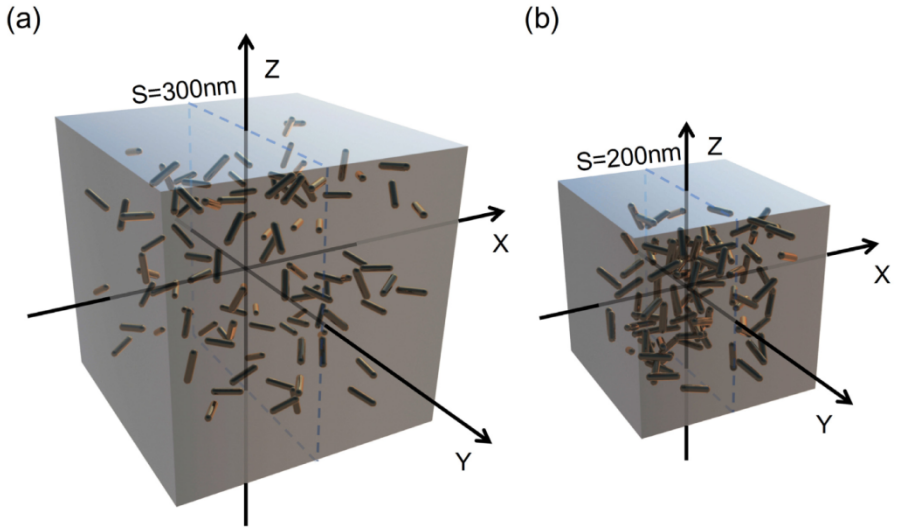

Fig. 1. Physical models for GNR clusters without (a) and with (b) plasmonic coupling between GNRs. The volumes of the boxes in which 100 GNRs with random orientations and positions are enclosed are 300 × 300 × 300 nm^3 (a) and 200 × 200 × 200 nm^3 (b), respectively.

The normalized linear and nonlinear absorption spectra calculated for the GNR cluster with negligible plasmonic coupling is shown in Fig. 2(a). At each wavelength, the electric field distribution of the GNR cluster was firstly calculated. Then, the linear and nonlinear absorption of each GNR were derived by calculating the integration of $\kappa|E|^2$ and $|E|^4$ over the volume of the constituent GNRs, respectively. The linear and nonlinear absorption of the GNR cluster were obtained by summing up the linear and nonlinear absorption of all the constituent GNRs. Similar method has been previously employed to derive the linear and nonlinear absorption of GNRs [6,43,44].

Optics EXPRESS

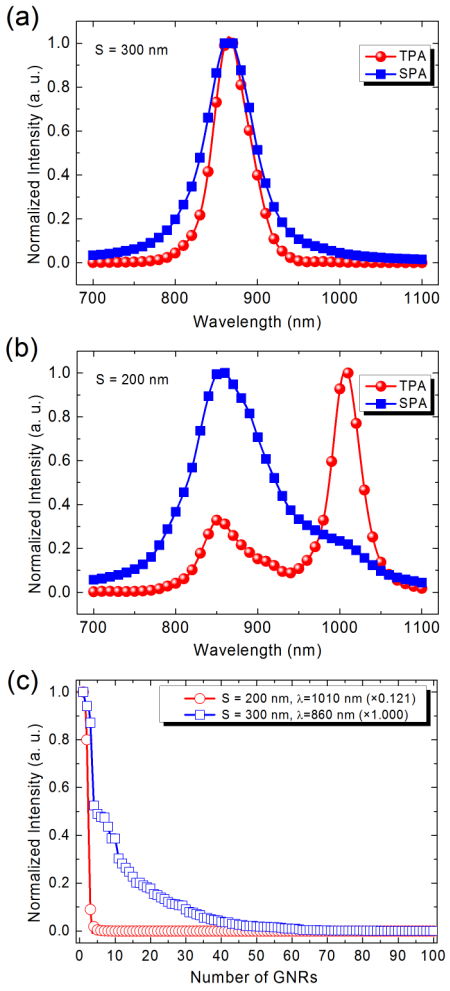

Fig. 2. Linear and nonlinear absorption spectra calculated for the GNR clusters containing 100 GNRs enclosed in a box with a volume of 300 × 300 × 300 nm^3 (a) and 200 × 200 × 200 nm^3 (b). (c) Normalized nonlinear absorption (or TPA) of the 100 GNRs in the two GNR clusters plotted in a descending order. The wavelengths of the incident light were chosen at the nonlinear absorption peaks of the corresponding GNR clusters (i.e., 860 and 1010 nm)

In Fig. 2(a), it can be seen that the linear absorption peak of the GNR cluster appears at ~860 nm, which is basically determined by the LSPR of the constituent GNRs in the absence of plasmonic coupling. It is noticed that the nonlinear absorption peak appears at the same wavelength. When plasmonic coupling is introduced into the GNR cluster, both linear and nonlinear absorption are modified, as shown in Fig. 2(b). In this case, the linear absorption peak remains nearly unchanged. However, the absorption band is broadened with a shoulder emerging at ~1010 nm. More interestingly, the nonlinear absorption peak is separated from the linear one and red shifted to ~1010 nm. The physical mechanism responsible for the separation of the linear and nonlinear absorption peaks has been described in detail in a previous publication [39]. Basically, multiple absorption peaks begin to appear in the linear and nonlinear absorption spectra of GNRs once the plasmonic coupling is introduced. For strong plasmonic coupling, the nonlinear absorption spectrum of the GNR cluster becomes dominated by the absorption peak at the long wavelength side of the LSPR. It is because that the nonlinear absorption is proportional to $|E|^4$ and the stronger electric field leads to a larger red shift in the absorption peak. In Fig. 2(c), we present the statistics for the nonlinear

Optics EXPRESS

absorption of the 100 GNRs in the two GNR clusters. It can be seen that the nonlinear absorption of the GNR cluster with strong plasmonic coupling is dominated by a few GNRs with significantly enhanced TPA. In the GNR cluster with plasmonic coupling, the TPA of the GNR with the largest value is enhanced by a factor of ~8.3 as compared with that of the isolated GNR with the largest value, as shown in Fig. 2(c).

3.2 Enhanced temperature rise in GNR clusters

Understanding the heat generation and temperature rise in GNR clusters is crucial for the photothermal therapy of single cells mediated by the naturally created GNR clusters. Upon the irradiation of fs laser light, a transition of electrons from the *d* band to the *sp* conduction band of Au can be induced in GNRs by simultaneously/sequentially absorbing two photons [45–48]. Heat is generated when hot electrons relax from the high-energy states to the low-energy states just above the Fermi level. The recombination of the relaxed electrons with the holes left in the *d* band may occur by emitting either photons (i.e., TPL) or photons (heat generation). Therefore, the photothermal conversion efficiency is determined mainly by the nonlinear absorption of GNR clusters which enhances light harvest and heat generation. For isolated GNRs, it depends strongly on the size and aspect ratio of GNRs and the wavelength of the excitation laser. For GNR clusters, it may be affected by the number of GNRs in the cluster, the plasmonic coupling between GNRs and the wavelength of the excitation laser. Therefore, it is a big challenge to accurately determine the photothermal conversion efficiencies (i.e., the conversion efficiency of laser energy to heat) for isolated GNRs and GNR clusters from the experimental point of view.

In order to gain a deep insight into the effects of plasmonic coupling on the nonlinear absorption and heat generation of GNR clusters, we have simulated the temperature distributions induced in the two GNR clusters discussed above by a plane wave with the same power. The simulated temperature distributions on the central planes (YZ planes) for the two GNR clusters are presented in Figs. 3(a) and 3(b), respectively. In the numerical simulation, it is assumed that the heat released by each GNR in the cluster is proportional to the nonlinear absorption of the GNR. By comparing the temperature distributions shown in Figs. 3(a) and 3(b), it can be seen that the temperature rise achieved in the GNR cluster with plasmonic coupling is much larger than that in the GNR cluster without plasmonic coupling. Apart from the significantly enhanced nonlinear absorption induced by the strong plasmonic coupling, it is thought that the heat accumulation, which becomes more significant when the mean distance between GNRs (i.e., heat sources) is reduced, also contributes to the large temperature rise.

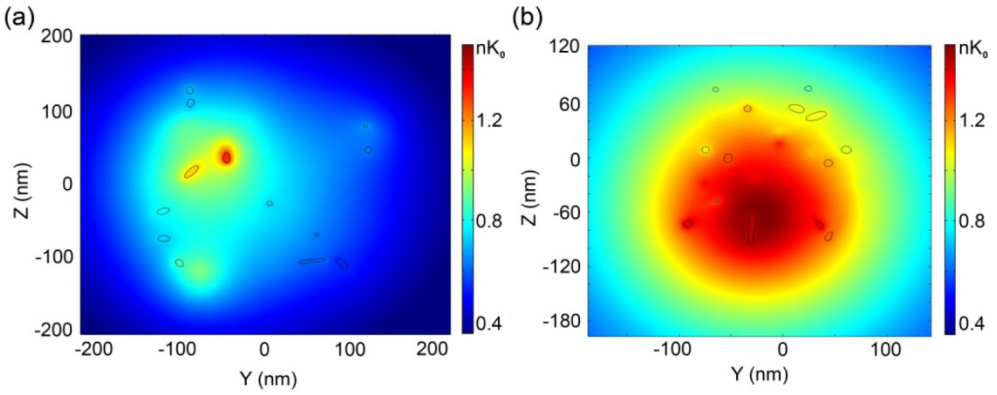

Fig. 3. Two-dimensional temperature distributions on the YZ plane simulated for the two GNR clusters without (a) and with (b) plasmonic coupling which are shown in Figs. 1(a) and 1(b), respectively. The black circles represent the cross sections of the GNRs on the YZ plane.

Optics EXPRESS

3.3. Morphology, absorption, cytotoxicity and uptake of GNRs

The morphology of the GNRs synthesized by using the modified seedless method was examined by using TEM observation, as shown in Fig. 4(a). The averaged length and diameter of the GNRs were estimated to be 34 and 8 nm, respectively. In Fig. 4(b), we show a typical absorption spectrum measured for GNRs dispersed in water. It can be seen that the LSPR and transvers surface plasmon resonance (TSPR) of the GNRs appear at 800 and 530 nm, respectively. The wavelength of the LSPR is in good agreement with that simulated by using the FDTD method (not shown).

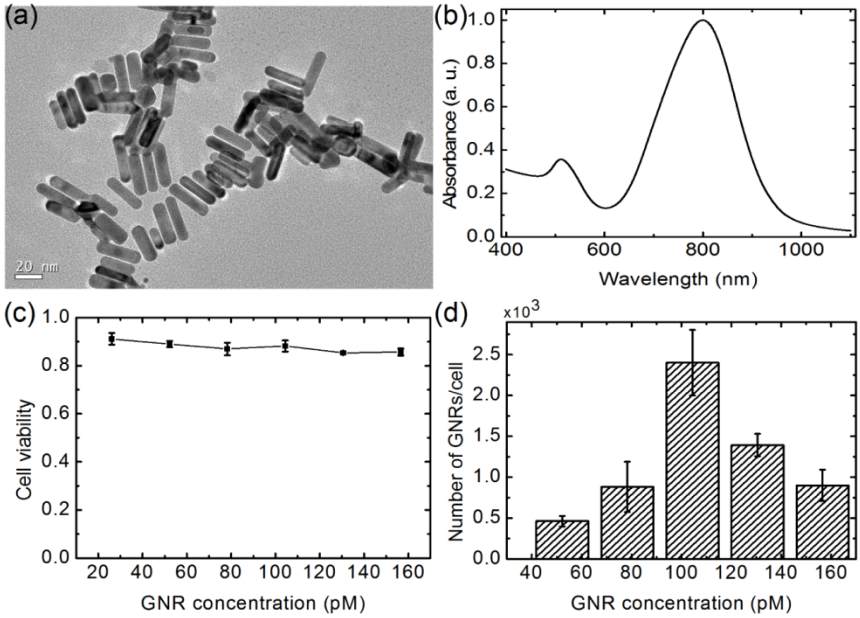

Fig. 4. (a) TEM image of the synthesized GNRs. (b) Absorption spectrum of the GNRs dispersed in water. (c) Cytotoxicity of GNRs against HepG2 cells. (d) Uptake of the GNRs measured for HepG2 cells.

The cytotoxicity of the GNRs to HepG2 cells was examined by doping the culture media with the GNRs of different concentrations ranging 0 to 150 pM and incubating HepG2 cells with the culture media for 24 hours. The viability of HepG2 cells, which was assessed by a MTT assay, as a function of the GNR concentration is shown in Fig. 4(c). It is noticed that for the highest concentration of GNRs, the viability of HepG2 cells was still higher than 80%. It implies that the GNRs are almost nontoxic to HepG2 cells if the concentration of the GNRs is not too large.

In order to realize efficient photothermal therapy, the uptake of the GNRs for HepG2 cells was also studied. Interestingly, it was found that the uptake of the GNRs is not proportional to the concentration of the GNRs. Instead, it exhibits a dependence on the concentration of the GNRs, as shown in Fig. 4(d). The maximum uptake of the GNRs, which was estimated to be ~2400 GNRs per cell, is observed at a GNR concentration of ~100 pM. The behavior is attributed to the returning of GNRs from HepG2 cells into the culture media after some time. Since the efficiency of photothermal therapy is closely related to the number of GNRs entering into cells, the optimum GNR concentration of ~100 pM was used in the photothermal therapy experiments described in the following.

Optics EXPRESS

3.4 GNR clusters formed in lysosomes

It has been known that the GNRs entering into cells are generally encompassed in the lysosomes, forming GNR clusters. This behavior offers us the opportunity to perform photothermal therapy for single HepG2 cells with ultralow pulse energy because the GNRs clusters can effectively convert the energy of photons into heat, leading to a high temperature. We first examined the accumulation of GNRs in the lysosomes of HepG2 cells by using TEM observation. The samples prepared for the TEM measurements have been described in Section 2. In Fig. 5(a), we show the TEM image for one of the lysosomes in a HepG2 cell which has been cultured with GNRs for 24 hours. From the magnified TEM image shown in Fig. 5(b), one can see clearly a GNR cluster containing ~30 GNRs with random orientations. The total dimension of the GNR cluster was estimated to be ~150 nm. However, it is remarkable that the reshaping of GNRs occurred when they expose to complex biological environments after entering into cells. It suggests that the surface of GNRs has not been successfully passivated by PEG, which is also reflected in the slight reduction of cell viability with increasing concentration of GNRs shown in Fig. 4(c). It is also noticed that the number of GNRs distributed outside the lysosomes is quite small, confirming that most GNRs entering into HepG2 cells are enwrapped into lysosomes. No GNRs were found in the nucleus of the cell.

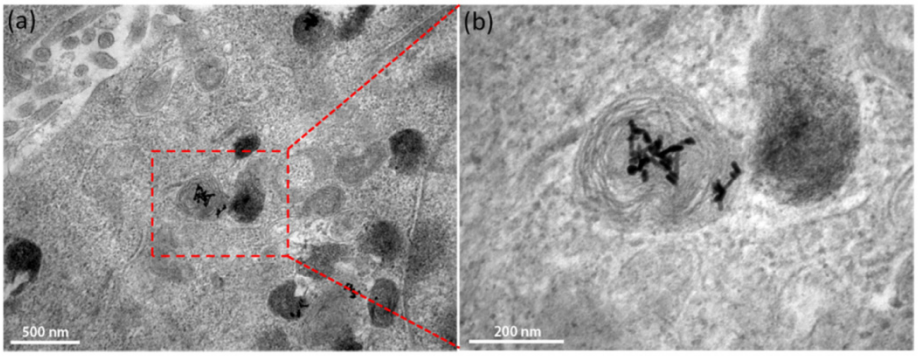

Fig. 5. (a) TEM image of a HepG2 cell which has been cultured with GNRs for 24 hours. (b) TEM image of a GNR cluster naturally created in the lysosome of the HepG2 cell.

As discussed in Section 3.1, GNR clusters with strong plasmonic coupling are expected to emit stronger TPL as compared with isolated GNRs or GNR clusters with negligible plasmonic coupling. For this reason, one can readily determine the locations of such GNR clusters by scanning the TPL image over the cell with fs laser light of low pulse energy. In this case, the heat released by GNR clusters is too small to affect the cell. In Fig. 6, we compare the TPL images for HepG2 cells without and with GNR clusters. For HepG2 cells not incubated with GNRs, on obvious TPL could be detected and the TPL image appeared to be dark. In comparison, apparent TPL could be observed in HePG2 cells which had been incubated with GNRs for 24 hours. In this case, it is noticed that the regions with strong TPL appear in the cytoplasm next to the nucleus (i.e., lysosomes), in good agreement with appearance of the GNR clusters observed in the TEM images.

Optics EXPRESS

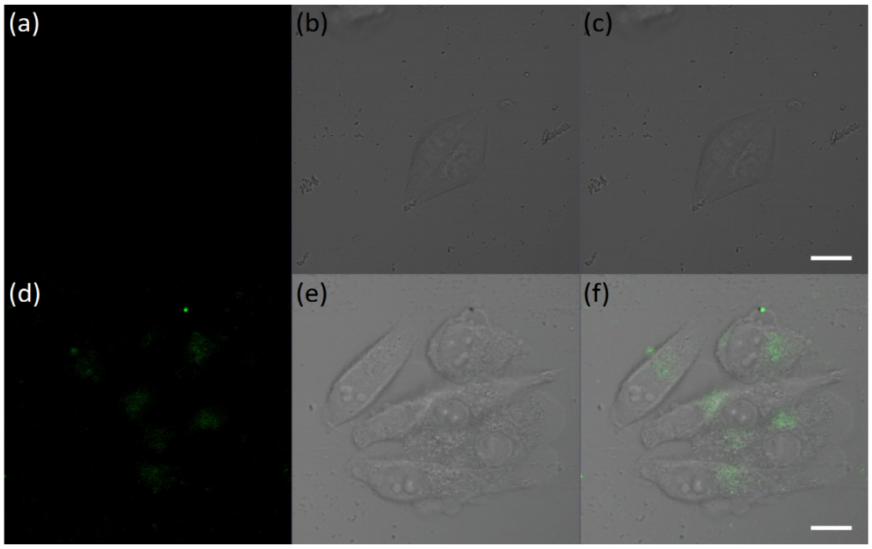

Fig. 6. TPL and bright field images recorded for HepG2 cells not incubated with GNRs [(a) and (b)] and incubated with GNRs [(d) and (e)]. The merged images for the two types of HepG2 cells are shown in (c) and (f), respectively. The length of the scale bar is 20 μm.

3.5 Photothermal therapy mediated by GNR clusters

Different from the previous studies on GNR-based photothermal therapy, we investigated the photothermal therapy of single cells by exploiting the enhanced TPA/TPL in GNR clusters. In this case, one can reduce the excitation spot of the fs laser light to a small diameter of a few micrometers by using an objective lens with a large NA. In this way, the photothermal therapy of single cells with ultralow pulse energy and short time can be realized.

Once the locations of GNR clusters in a single cell are determined with the help of TPL images, one can carry out photothermal therapy for the cell by simply exciting the GNR cluster with the large TPA/TPL with a higher pulse energy. In this way, accurate and rapid injury to cancer cells can be easily achieved. Generally, bubbles generated by laser heating of GNR clusters can be observed, implying that the temperature at the focal point can exceed the boiling point of water. In this case, the high temperature will lead to the apoptosis of HepG2 cells in a short time of a few seconds.

In Fig. 7, we show the evolution of the morphology of a HepG2 cell during the photothermal therapy process. Figure 7(a) shows the bright field image of the chosen cell. Figures 7(b)-7(l) show the cellular morphology together with the TPL image when the cell was exposed to the laser light in different times. It was found that several bubbles began to appear at different places where the GNR clusters with large TPA were located. With increasing irradiation time, the bubbles become larger and the cell shape was deformed. In this case, the HepG2 cell suffered from morphological damage as the bubbles expanded.

Optics EXPRESS

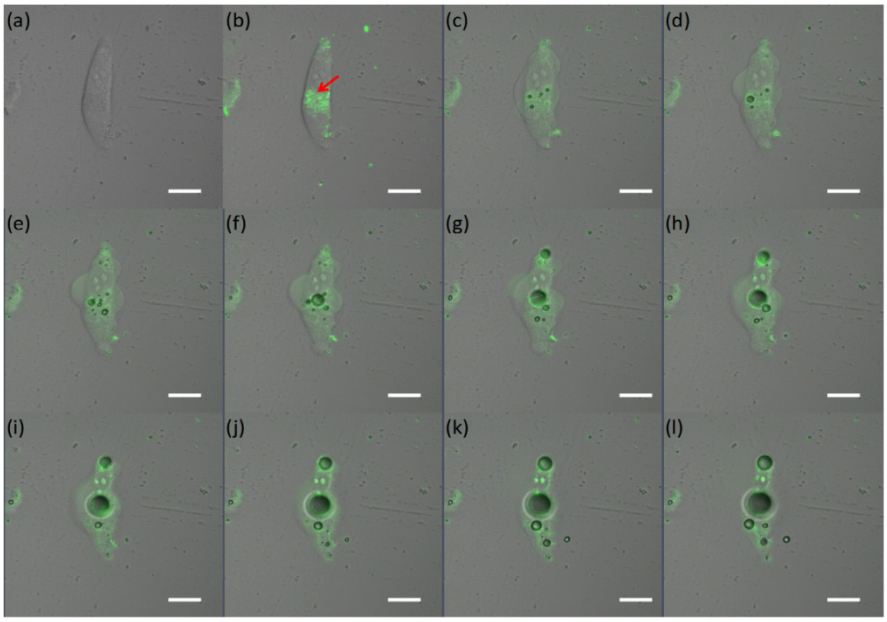

Fig. 7. (a) Bright field image of the chosen cell. (b)–(l) Evolution of the cell morphology and TPL image when the cell was exposed to the fs laser light in different time of 0, 0.1, 0.2, 0.3, 0.4, 0.5, 0.6, 0.7, 0.8, 0.9 and 1.0 s, respectively. The length of the scale bar is 20 μm.

In the above experiments, a laser beam from a confocal laser scanning microscope with pulse energy of ~35 pJ was firstly used to obtain the TPL image of the targeted cell from which the location of the GNR cluster with the largest TPA could be located. Then, another laser beam with larger pulse energy of ~420 pJ was focused on the GNR cluster while the rapid scanning of the cell was performed by using the weaker laser beam with pulse energy of ~35 pJ. It can be seen that a bubble emerged firstly at the location of the GNR cluster with the largest TPA. Although the pulse energy used for scanning was intentionally chosen to be low, small bubbles began to appear at other places after many times of scanning. In Fig. 7(c), one can identify four bubbles with different volumes. More bubbles begin to emerge when the irradiation time is increased, can be seen in Fig. 7(e). It is also observed that the largest bubble at the center part of the cell expanded rapidly.

The photothermal therapy can also be performed by exciting only a single GNR cluster without scanning the whole cell. As shown in Fig. 6(f), it is easy to find the location of the GNR cluster with the largest TPA based on the TPL image obtained by using low pulse energy. It is expected that the most effective photothermal therapy can be realized by exciting such a GNR cluster. In Figs. 8(a) and 8(b), we show the morphology change observed for a HepG2 cell before and after the photothermal therapy performed with pulse energy of 192 pJ. One can see the appearance of a bubble and the apparent deformation of the targeted cell after an irradiation time of only 3 s. The evolution of the TPL spectrum during the photothermal therapy process was also recorded, as shown in Fig. 8(c). It can be seen that the TPL spectrum of the GNR cluster appears to be quite similar to that of GNRs and the TPL intensity increases with increasing irradiation time.

In the photothermal therapy experiments described above, the heat released by the GNR clusters is quite large, leading to a large temperature rise and bubble formation. In this case, a significant change in the morphology of the cells occurs which may lead to the necrosis of the cells. This situation may not be appropriate for practical applications. For this reason, we also used much lower pulse energy for the photothermal therapy of HepG2 cells and investigated

Optics EXPRESS

the dependence of the apoptosis time on the irradiation pulse energy at a fixed irradiation time of 20 s, as described in the following.

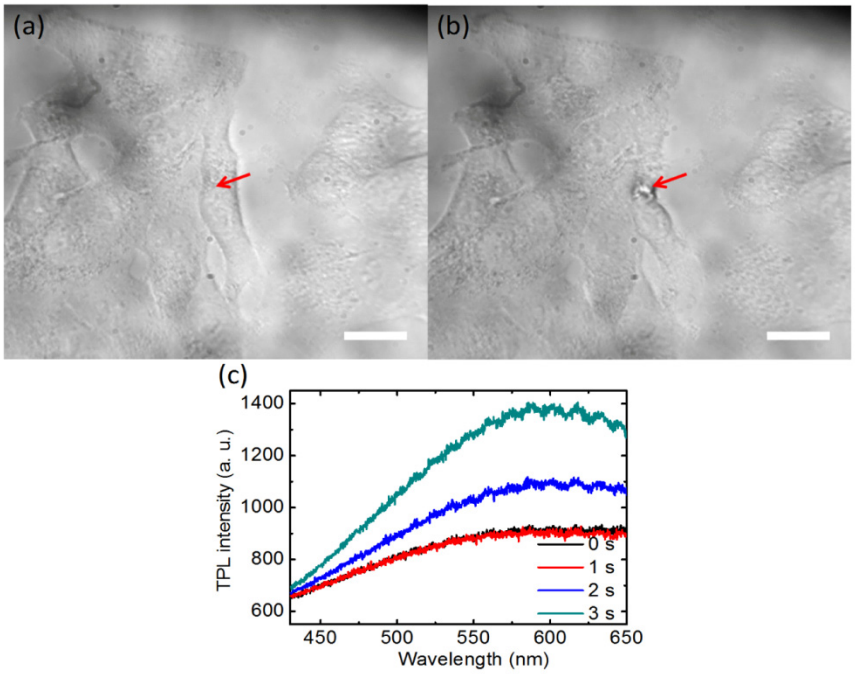

Fig. 8. HepG2 cells before (a) and after (b) photothermal therapy. (c) Evolution of the TPL spectrum of the excited GNR cluster during the photothermal therapy. The length of the scale bar is 20 μm.

Similar to the procedure described above, we first located the most efficient excitation spot of the targeted cells based on the TPL images obtained by using low pulse energy. Then, the targeted cells were exposed to the fs laser light with different pulse energies for 20 s. After that, the cells after photothermal therapy were dyed with Trypan Blue, which is a typical dye used to characterize the integrity of cell membrane and the survival rate of cells, after incubation in cell medium for different times of 0, 0.5, 1.0, and 2.0 hours. The damaged cells appear blue because of the increased permeability of the cell membranes and they are getting necrotic or late apoptotic. The results of the photothermal therapy for HepG2 cells are presented in Fig. 9. The grey images are the bright images of the cells before laser irradiation and the color ones are the images stained by Trypan Blue. It can be seen that only the positions irradiated with laser light appear blue while the colors of the rest parts remain unchanged. Since the apoptosis of the cells is indicated clearly by the change of color, it is noticed that the apoptosis time of the irradiated cell depends strongly on the pulse energy of the laser light, which is summarized in Fig. 10. It is noticed that the use of pulse energy of ~157 pJ leads to the necrosis of the cell. When the pulse energy is reduced to ~122 pJ, however, the death time is prolonged to about half an hour. For pulse energy as low as ~70 pJ, the membrane can still keep integrity for ~2 hours after the irradiation of the laser light. The finite survival time indicates that the cells after the photothermal therapy can receive certain biological operation because of the integrity of the cell membrane.

Optics EXPRESS

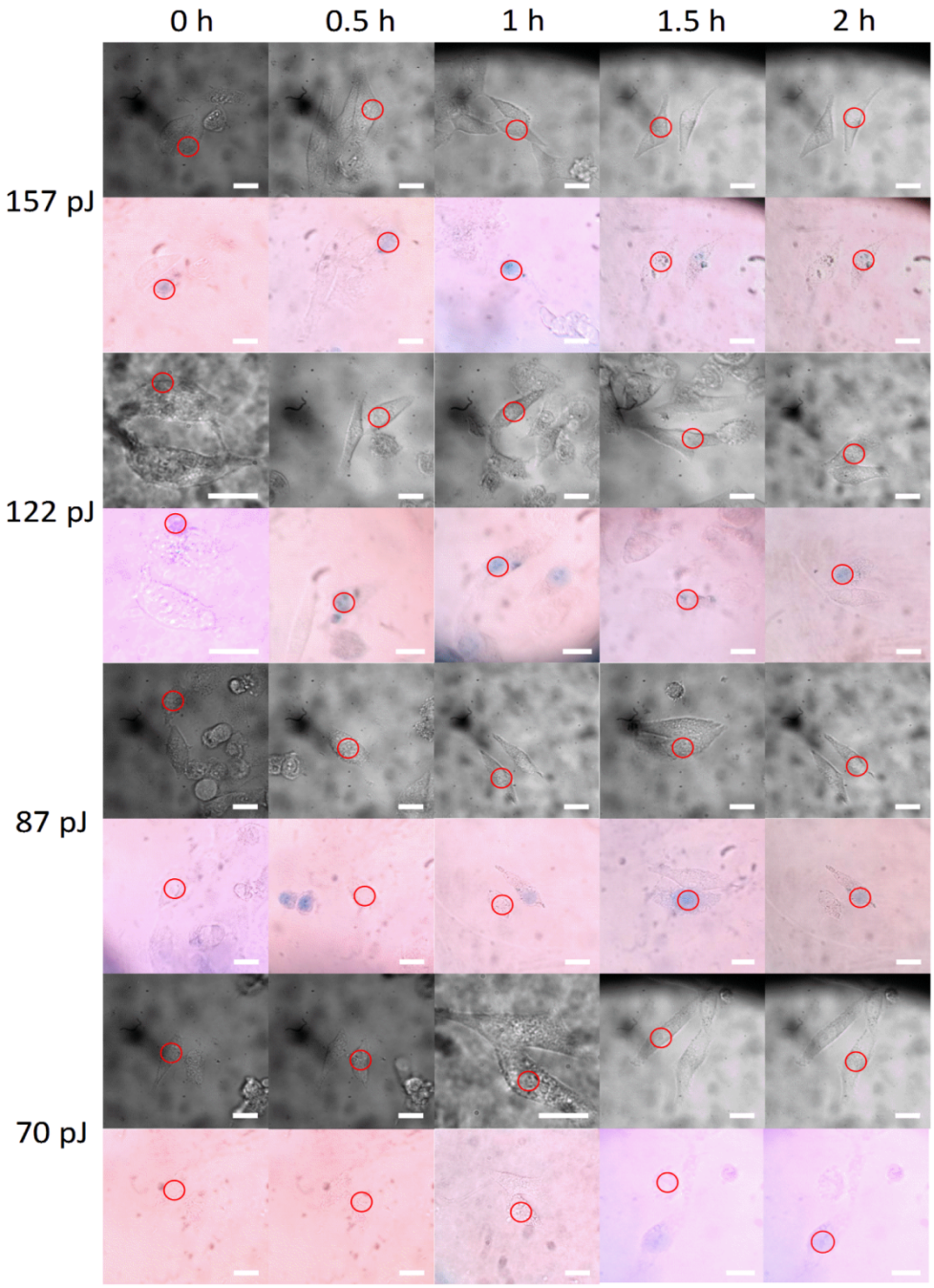

Fig. 9. Bright field images of the cells on which the photothermal therapy were carried out (black and white images). The color images show the cells dyed with Trypan Blue after the photothermal therapy. Laser light with different pulse energies of 157, 122, 87, and 70 pJ was employed in the photothermal therapy experiments. The cells after the irradiation of the laser light were dyed with Trypan Blue after different interval times of 0, 0.5, 1.0, and 2.0 hours. The length of the scale bar is 20 μm. The blue color appearing in some areas without dead cells is caused by Trypan Blue which did not diffuse uniformly in the experiment. For pulse energy of 87 pJ, there were occasionally two dead cells near the targeted cell on which the photothermal therapy was carried out.

Optics EXPRESS

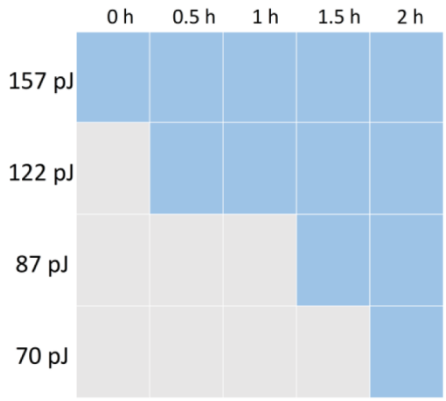

Fig. 10. Dependence of the apoptosis time of the HepG2 cells on the pulse energy of the irradiation light for a fixed irradiation time of 20 s.

4. Conclusion

In summary, we have investigated the photothermal therapy of single HepG2 cells mediated by the GNR clusters naturally formed in the lysosomes of the HepG2 cells. Based on the FDTD numerical simulation, it was revealed that both the TPA and the TPL of the GNR clusters formed in the lysosomes of HepG2 cells are significantly enhanced as compared with isolated GNRs or GNR clusters without plasmonic coupling. The enhanced nonlinear absorption leads to a larger temperature rise which can be utilized to induce the apoptosis of single cells. It was found that the locations of such GNR clusters can be easily identified based on the TPL images of single cells obtained by using low pulse energy. The excitation of such GNR clusters with fs laser light resulted in the change of cell morphology and the generation of bubbles, leading to the necrosis of the irradiated cells. In addition, it was found that the apoptosis of the cells can be induced by pulse energy as low as 70 pJ. The strong dependence of the apoptosis time on the pulse energy of the irradiation light was observed. Our findings are helpful for the photothermal therapy of single cancer cells with low pulse energy and will find potential application in biophotonics and biomedicine.

Funding

National Natural Science Foundation of China (Grant No. 11374109, 11674110, 61201102); Natural Science Foundation of Guangdong Province, China (Grant. No. 2016A030308010); Science and Technology Planning Project of Guangdong Province, China (Grant No. 2015B090927006).